Parametric study of chiral metamaterial structures for enhancing radiation characteristics of planar antennas

Oscar Fernández Fernández, Álvaro Gómez Gómez, Angel Vegas García

oscar.fernandez@unican.es, alvaro.gomez@unican.es, angel.vegas@unican.es.
Dpto. de Ingeniería de Comunicaciones. Universidad de Cantabria.
Plaza de la Ciencia s/n, 39005 Santander.

Abstract- **Chiral Metamaterials are artificial composite materials exhibiting further properties neither observed in its constituents nor available in the nature, such as negative refractive indices or high polarization plane rotations, or enhancing the composite features relative to the individual properties of its constituents. In this communication a comparative parametric study of different plane chiral metamaterials presenting 3D chirality is performed. The obtained results show how rosette-type structures are more appropriate to improve the rotation of the polarization plane whereas specular-type assemblies are more suitable for obtaining broader band widths. Finally, the application of these structures as antenna plane covers for enhancing the antenna gain and axial ratio is also examined.**

I. INTRODUCTION

Metamaterials allow the development of new composite structures exhibiting several properties available in the nature or enhancing considerably the features of its constituents. A typical example of these remarkable characteristics is the negative refractive index, which can be obtained through the superposition of two media that present simultaneously negative permeability and permittivity in a certain frequency band. Moreover, Pendry in [1] demonstrated that an artificial chiral media, besides producing optical activity, could also exhibit negative refractive index under certain conditions. It is worth of mention that the existence of natural chiral materials and their optical activity are known since 1848 [2]. But what is new and important about chiral metamaterials (CMM) is that the circular birefringence generated by them can reach to high values of the polarization plane rotation angle, around $250°/\lambda$ versus $0.02°/\lambda$ achievable by quartz.

Regarding to CMMs, there are several techniques for its manufacturing, such as the traditional one, wherein helical inclusions are dispersed in a dielectric host medium [3], and the latest technique, based on the Printed Circuit Board Technology [4]. The CMMs implemented according to the last technique are characterized by its designability, manufacturability and easiness of characterization using commercial software.

In this communication a comparative study, focused on the variation of the rotation angle of the polarization plane versus different geometric parameters is performed. Furthermore, the features of the CMMs are exploited in order to modify and improve the radiation characteristics of a microstrip patch antenna designed for operating at W-band by placing a CMM cover.

II. PLANE CHIRAL METAMATERIALS

A. Structures under analysis

Along this work several planar structures implemented in PCB and exhibiting 3D chirality will be analyzed.

The first set of structures, called mutual twist structures, is composed of chiral [4] (Fig. 1a) or achiral [5] (Fig. 1b) designs, presenting C_4 symmetry geometry, which are printed on both sides of the PCB with a relative twist between faces.
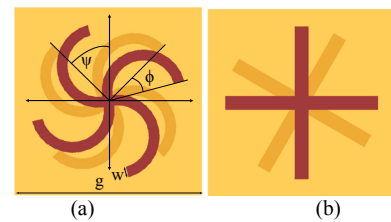

Fig. 1. Schematic of mutual twist type structures:
(a) rosettes [4] and (b) crosses [5].

The second set of assemblies, called specular structures, are designs exhibiting a 2D chiral C_4 symmetry structure on one side of the PCB and its enantiomer, with or without rotation, on the other side (Fig. 2).
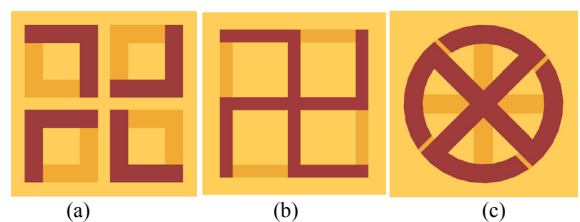

Fig. 2. Schematic of specular structures: (a) "L-shaped" [6], (b) conjugated gammadion [7] and (c) wheel [8].

Finally, the third sort of structures is composed of designs called "layer by layer" which are characterized by their manufacturability (Fig. 3) [9].
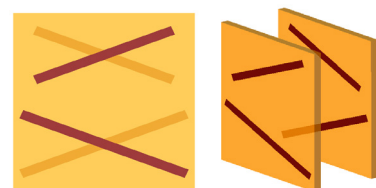

Fig. 3. Schematic of layer by layer structure [9].

B. Structures characterization

Applying the parameter retrieval algorithm published in [10] the aforementioned structures are characterized. Briefly, the procedure consists on impacting with a linearly polarized plane wave on the CMM structure under study and, afterwards, measuring the copolar and crospolar components of both reflected and transmitted fields. Then, the transmission and reflection coefficients are calculated and processed by applying the Jones matrix method [11]. Thus, the transmission (t_{++} and t_{--}) and reflection ($r_{++} = r_{--} = r$) coefficients of both right- (+, RHCP) and left- (-, LHCP) handed circularly polarized waves are obtained. In the notation of t_{++}, the first subscript indicates the circular polarization type of the transmitted wave, and the second one the circular polarization type of the incident wave.

The optical activity introduced by the chiral medium generates a rotation of the polarization plane (circular birefringence) (θ) and a distortion of the wave polarization, quantified by the ellipticity (η) of the polarization, which can be calculated from

$$\theta = -\frac{1}{2}\left[\arg(t_{++}) - \arg(t_{-})\right] \qquad (1)$$

$$\eta = \frac{1}{2}\tan^{-1}\left(\frac{|t_{++}|^2 - |t_{--}|^2}{|t_{++}|^2 + |t_{--}|^2}\right) \qquad (2)$$

Furthermore, the normalized impedance of the medium and the refractive index for both RHCP (n_+) and LHCP (n_-) waves are obtained by substituting the measured transmission (t_{++}, t_{--}) and reflection (r) coefficients of the circular waves into

$$Z = \pm\sqrt{\frac{(1+r)^2 - t_{++}t_{--}}{(1-r)^2 - t_{++}t_{--}}} \qquad (3)$$

$$n_{\pm} = \frac{-i}{k_d d}\left\{\ln\left[\frac{1}{t_{\pm\pm}}\left(1 - \frac{Z-1}{Z+1}r\right)\right] \pm 2m\pi\right\} \qquad (4)$$

Assuming the $e^{j\omega t}$ time dependence, the sign of (3) and the value of the integer m are obtained under the following assumptions

$$\mathrm{Re}(Z) > 0 \ , \ \mathrm{Im}(n_{\pm}) < 0$$

After determining Z and $n_{\pm}$, the rest of the characteristic parameters of the whole structure can be obtained from

$$n = \frac{n_+ + n_-}{2} \qquad (5)$$

$$\varepsilon = \frac{n}{Z}, \quad \mu = nZ \qquad (6)$$

$$\kappa = \frac{n_+ - n_-}{2} \qquad (7)$$

C. Parametric study

As it was previously mentioned, besides the possibility of exhibiting negative refractive index, the main difference between the conventional chiral materials and the new CMMs is the high values of the polarization plane rotation that the latter structures can produce. Therefore, in order to carry out the parametric study, the dependence of the geometric characteristics of the structure on the rotation of the polarization plane will be analyzed.

Among the aforementioned structures, as an example, we will focus our attention in the rosette geometry. Thus, Fig. 4 shows the variation of θ versus frequency for different values of its most significant parameters: relative twist angle (ϕ), line width (w), and unit cell base rotation angle (ψ) and side length (g).
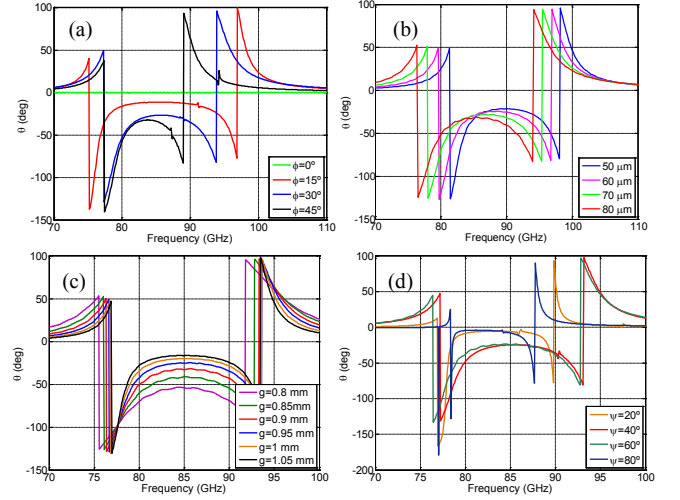

Fig. 4. Variation of the polarization plane rotation angle versus frequency for the structure of Fig. 1a for several values of (a) relative twist angle, (b) line width, (c) unit cell side length and (d) unit cell base rotation angle.

Regarding to this structure, it is important to note that its 3D chirality is due to the relative twist (ϕ) existing between the stamps of each face. This fact can be inferred from Fig. 4a, wherein the variation of θ versus frequency is plotted for several values of ϕ. Here, it can be seen that for $\phi = 0$ the structure is achiral, i.e., there is no rotation of the polarization plane. In contrast, when ϕ is increased the CMM sample does show chirality. In addition, when $\phi = 45°$ the rotation of the polarization plane reaches to its maximum value $\theta = -32°$.

Moreover, inspecting Fig. 4b it can be seen that an increasing of the line width (w) produces an enlarging of the rosette electrical length and, consequently, a reduction of the operating frequency. Furthermore, the increasing of w also produces a higher value of θ, shifting from $-20°$ with w = 50 μm to $-31°$ with w = 80 μm.

At this point, it is worth of mention that the chirality exhibited by the CMM is not only associated with the pattern itself (geometry, relative twist and line width) but also with the arrangement of the pattern (unit cell base rotation angle and side length) on the PBC. These effects can be seen in Figs. 4c and 4d, wherein the variation of θ versus frequency for different values of g and ψ are shown, respectively.

Fig. 4c shows than when the unit cell length size is increased (for example, from g = 0.8 mm to 1.05 mm), the separation between the metallization of neighboring cells enlarges and, as a result, θ is reduced, decreasing from $-56°$ to $-16°$.

In a similar way, the rotation of both rosettes in the unit cell (ψ) (Fig. 1a) also determines the separation of adjacent geometries, as the distance between neighboring rosettes will differ. From Fig. 4d, it can be extracted that a very high or a very low ψ value (around 80º or 20º), produce low values of θ, almost 0. However, when ψ is shifted to an intermediate value ($\psi = 40$ º) the bandwidth increases and the value of θ is also enlarged (20-25°).

Although the aforementioned results correspond to a specific structure, analogous results can be obtained with the other structures introduced in the previous section (Figs. 2 and 3). In order to go further in our analysis, the behavior of the structures within the same set has been compared. Thus, Fig. 5 presents the variation of θ versus frequency for each group of assemblies. For all cases the Rogers RO3003 dielectric with ε_r = 3, tg δ = 0.0013 and 5 mils (127 μm) thickness is used. In Fig. 5a the rotation produced by the mutual twist type structures (Fig. 1) for two different relative twist angles, ϕ = 15º and ϕ = 30º, is displayed. It can be seen that, for the same ϕ and dielectric thickness, the crosses provide a greater rotation of the polarization plane than the rosettes do. In particular, for ϕ = 30º the rotation angle produced by the crosses doubles the one obtained with the rosettes. However, the rosettes exhibit the advantage of featuring a more compact geometry (smaller unit cell), allowing a greater number of rosettes per unit area than crosses. In our analysis the rosettes unit cell has a side length of 0.96 mm while the crosses one has a side length of 1.12 mm.
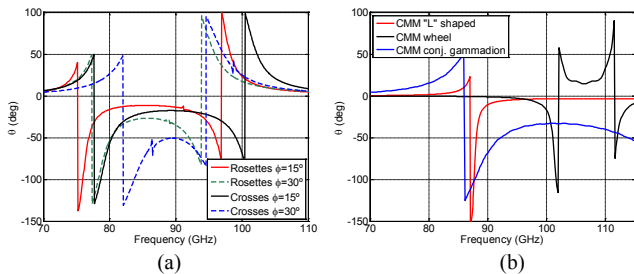

Fig. 5. Variation of the polarization plane rotation angle versus frequency for several (a) mutual twist type and (b) specular type structures.

Figure 5b shows the rotation angle of the polarization plane produced by the specular structures (Fig. 2): L-shaped pattern, conjugated gammadion and wheel. By comparing the three curves, a very different behavior is observed among them. The L-shaped pattern presents a very low value of θ for the given dielectric thickness. Meanwhile the conjugated gammadion CMM provides the highest value of θ (θ = –33º) and a wide bandwidth wherein the θ remains, practically, constant. The wheel CMM produces an intermediate value of θ (θ = 15°) and a much narrower bandwidth than the conjugated gammadion pair does. Regarding to the unit cell length sizes, the wheel pair is the most compact structure, with a unit cell size of g = 0.6 mm side. On the other hand, the conjugated gammadion is slightly larger, g = 0.69 mm, for the L-shaped CMM g = 1.29mm, being the largest one.

Finally, the third type of structure analyzed is the layer by layer geometry (Fig. 3), which most attractive features are its simple geometry, manufacturability, and its reciprocity. In contrast, this structure presents the drawback of needing a "great" separation between both layers, making it unsuitable for some applications, such as the one presented in Section III. Regarding to its chirality, it produces a polarization rotation angle of θ = 55 º.

From the analyzed structures, the two geometries exhibiting the best relation between the unit cell size and rotation are the rosettes and the conjugated gammadion CMM. On the one hand, the geometry of the conjugated gammadion provides a reciprocal response and is more compact than the rosette one, allowing a higher density. On the other hand, the rosette, despite its larger unit cell side and asymmetric transmission, provides a larger rotation angle.

III. ANTENNAS ENHANCING

An important property exhibited by the chiral structures is their ability to focus the rays passing through the structure [12]. In this section this feature is used for improving the radiation characteristics of a microstrip patch antenna in the W-band by placing a flat chiral metamaterial (with rosette pattern) cover above it (see Fig. 6a).
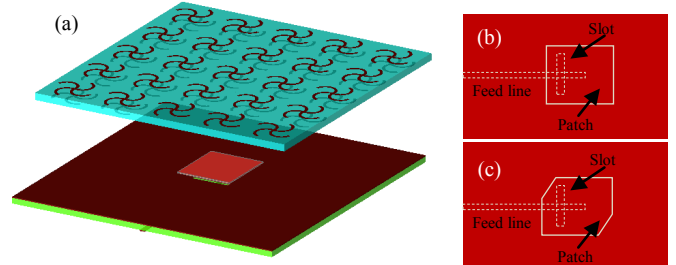

Fig. 6. Microstrip patch antenna with CMM cover (a). Patch antenna with linear polarization (b) and elliptical polarization (c)

The separation between the patch antenna and the cover is critical in the performance of the radiating structure. Experimentally it has been found that the best measurements for the antenna gain and the S_{11} parameter are obtained when this distance is around 1.6 mm.

Next, the antenna gain versus frequency is analyzed. For this purpose, two different slot coupled patch antennas are used: (i) a rectangular patch with linear polarization, Fig. 6b, and (ii) the same patch with two chamfered corners (corner-cuts) (Fig. 6c) that provides elliptical polarization. Fig 7 shows the antenna gain (total gain) and the LH and RH circular component gains of both antennas (with and without cover). On inspecting Fig. 7, the covered antennas responses show two regions with different performances. In the first one, 88-98.5 GHz, we find a higher gain in comparison with the uncovered patch antenna, and very similar responses of the RH and LH components. This gain enhancement is due to the effective antenna surface increase, but it is not related to the chirality of the structure.
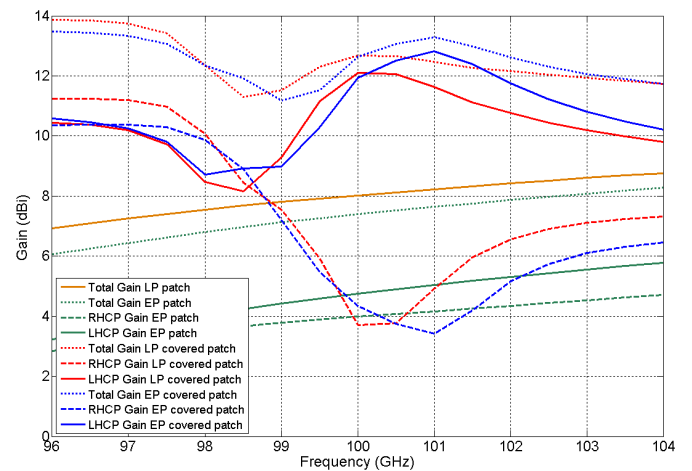

Fig. 7. Antenna gain (total gain) and the gain of the LH and RH circular components of both patch antennas with and without cover. LP and EP stand for linear and elliptically polarizations, respectively.

The second region, starting around 98.5 GHz, reflects the chirality of the cover, as different gains for RHCP and LHCP components are obtained for both covered antennas.

For the rectangular patch antenna with cover, the measured gains are 12 dBi for the LHCP component and 4 dBi for the RHCP one, at 100 GHz. This gain contrast, 8dB, highlights the different absorption degrees on both circular components (circular dichroism), and determines the type of polarization of the resulting signal. The axial ratio (AR) quantifies the polarization type of the resulting field. The polarization is circular when $|AR| < 3$ with a pure circular polarization when $|AR| = 1$.

In Fig. 8, the axial ratio in the broadside direction versus frequency for the structure of Fig. 6b is depicted. In the frequency band between 99.7 and 101 GHz, an $|AR| < 3$ is observed, indicating that the linear polarization of the field radiated by the microstrip antenna is transformed, through the CMM cover, from linear to circular polarization.

For the second antenna, Fig. 7 and 8 show the antenna gain and the axial ratio in the broadside direction for both uncovered and covered cases. From this figures, it can be seen that the uncovered antenna radiated field is not circularly polarized, since it shows slight differences between the RH and LH components and its axial ratio is high, AR > 16 in the entire band of interest.

When the cover is placed, the difference between the RHCP and LHCP component gains is significantly increased, reaching a maximum value of 9.5 dB at 101 GHz. Moreover, as shown in Figure 8, the axial ratio is improved considerably, obtaining $|AR| < 3$ (circular polarization) between 99.75 and 102.25 GHz.

Regarding to the CMM cover, it is important to note that its own geometry determines the RH and LH component responses. In Table I, the gain differences of the RH and LH component and the axial ratio for the rosettes and conjugated gammadion CMM structures are listed. The results show that the conjugated gammadion CMM cover provides greater difference between circular components (when the patch antenna is circularly polarized) and a greater bandwidth than rosettes CMM cover.

Table I. Maximum gain difference and frequency range with circular polarization.

Type of structure	Patch Polariz.	Max difference $|G_+-G_-|$	$|AR| < 3$
Rosettes	LP	8 dB @ 100 GHz	99.7 – 101 GHz
	EP	9.5 dB @ 101 GHz	99.75 - 102.25 GHz
Conjugated Gammadion	LP	7.3 dB @ 103.5 GHz	102.5 – 106 GHz
	EP	14.3 dB @103.5 GHz	101.75 – 108 GHz

IV. CONCLUSIONS

In this communication we have presented a comparative parametric study of several planar chiral metamaterial structures. It has been shown that the rosettes and the conjugated gammadion CMM exhibit the best relation between the unit cell size and the rotation of the polarization plane. The conjugated gammadion presents a compact geometry and a reciprocal response, whereas the rosette presents asymmetrical transmission and a larger rotation angle.

Finally, these CMM structures have been used for designing antenna covers which allow the implementation of circular polarized antennas from other simple antennas that

do not present this type of polarization. Moreover, the CMM cover can also improve the axial ratio of circular polarization antennas, approaching its AR to 1.
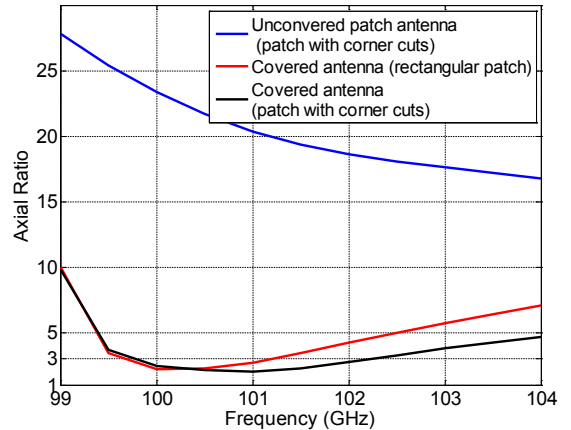

Fig. 8. Variation of the Axial Ratio versus frequency (Rosette pattern with patch antenna with circular and linear polarizations).

REFERENCES

[1] J. B. Pendry, "A chiral route to negative refraction", *Science*, vol. 306, no. 5700, pp. 1353-1355, Nov. 2004.
[2] Louis Pasteur: "Sur les relations qui peuvent exister entre la forme cristalline, la composition chimique et le sens de la polarisation rotatoire", *Ann. de Chim. et Phy.*, vol. 24, pp. 442–459, 1848.
[3] A. Gomez, A. Lakhtakia, J. Margineda, G. J. Molina-Cuberos, M. J. Nuñez, J. A. Saiz-Ipiña, A. Vegas, M. A. Solano, "Full-Wave Hybrid Technique for 3-D Isotropic-Chiral-Material Discontinuities in Rectangular Waveguides: Theory and Experiment," IEEE Trans. Microw.Theory Tech., vol. 56, no.12, pp. 2815-2825, Dec. 2008.
[4] E.Plum, J.Zhou, J.Dong, V. A. Fedotov, T.Koschny, C. M. Soukoulis, and N. I. Zheludev, "Metamaterial with negative index due to chirality," *Phys. Rev. B*, vol. 79, 035407, 2009.
[5] J. Zhou, J. Dong, B. Wang, T. Koschny, M. Kafesaki, and C. M. Soukoulis, "Negative refractive index due to chirality," *Phys. Rev. B*, vol. 79, 121104, 2009.
[6] J. Li, F. Q. Yang, and J. F. Dong, "Design and simulation of l-shaped chiral negative refractive index structure," *Progress In Electromagnetics Research*, vol. 116, 395-508, 2012.
[7] R. Zhao, L. Zhang, J. Zhou, Th. Koschny, and C.M. Soukoulis, "Conjugated gammadion chiral metamaterial with uniaxial optical activity and negative refractive index," *Phys. Rev. B*, vol. 83, 035105, 2011.
[8] Y. Ye, X. Li, F. Zhuang, and S. W. Chang, "Homogeneous circular polarizers using a bilayered chiral metamaterial," *Appl. Phys. Lett.*, vol. 99, 031111, 2011.
[9] L.Wu, Z. Y. Yang, Y. Z. Cheng, Z. Q. Lu, P. Zhang, M. Zhao, R. Z. Gong, X. H. Yuan, Y. Zheng, and J. Duan, "Electromagnetic manifestation of chirality in layer-by-layer chiral metamaterials," *Optics Express*, no. 5, 5239, 2013.
[10] R. Zhao, T. Koschny, and C. M. Soukoulis, "Chiral metamaterials: retrieval of the effective parameters with and without substrate," *Opt. Express*, vol. 18, no. 14, pp. 14553–14567. Jul 2010.
[11] C. Menzel, C. Rockstuhl, F. Lederer, "Advanced Jones Calculus for the classification of periodic metamaterials," *Phys. Rev. A*, vol. 82, no. 5, 053811, Nov. 2010.
[12] D.Zarifi, H. Oraizi, and M.Soleimani, "Improved performance of circularly polarized antenna using semi-planar chiral metamaterial covers," *Progress In Electromagnetics Research*, vol. 123, 337-354, 2012.